Parametric Study on the Dynamic Aeroelastic Analysis of a Two-Stage Axially Deploying Telescopic Wing

Sayed Hossein Moravej Barzani[1], Hossein Shahverdi[2*], Mohammadreza Amoozgar[3]

[1,2] *Department of Aerospace Engineering, Amirkabir university of Technology, Iran, Tehran*

[3] *Faculty of Engineering, University of Nottingham, Nottingham, NG7 2RD, United Kingdom*

Abstract

In this paper, the flutter instability of a conventional two-stage axially moving telescopic UAV wing is investigated. To this aim, and to be as close as possible to the reality, the effects of temporal variation of mass and length, due to the movement of stages and their overlapping, along with the effects of morphing speed are considered for the first time. The bending-torsional dynamics of the two-stage wing is modelled by modifying the Euler-Bernoulli beam theory to take into account the effects of morphing speed and variations of mass and length. Furthermore, the aerodynamic loads are simulated using Peters' unsteady aerodynamic model. The governing aeroelastic equations are discretized using a finite element approach, and a length-based stability analysis is proposed to investigate the aeroelasticity of the wing. The obtained results are compared with those available in the literature, and a good agreement is observed. It is found that the aeroelastic stability of a telescopic wing is more sensitive to the fixed part parameters than the moving part. Also, it is shown that the wing critical length is sensitive to the morphing speed. Therefore, by selecting the telescopic wing morphing parameters properly, the aeroelastic stability of the system can significantly be improved.

Keywords

Morphing aircraft, aeroelastic stability, unsteady aerodynamic, variable span wing, morphing speed.

Corresponding author, Email address: h_shahverdi@aut.ac.ir

1. Introduction

Due to their promising performance, morphing wings have received a huge interest in the past decade. Among all possible morphing concepts, the wing extension concept has been shown to be an effective method for improving both aircraft range and endurance (Friswell and Inman, 2006). However, as a result of the change in the wing dimensions, the dynamic characteristics of the system are altered. Thus, it is crucial to understand the dynamic behaviour of the wing when designing such structures.

Due to the nature and dimensions of UAV wings, the beam theory is mainly used to analyze the dynamics of slender wings (Bisplinghoff et al., 2013). Many researchers have studied the dynamic behaviour of axially moving beams. Wang and Wei (1987) studied the vibration of a robot arm modelled by a moving slender prismatic beam. In this study, it was shown that increasing or decreasing the length of the flexible arm has destabilizing or stabilizing effects on the arm vibrations. Stylianou and Tabarrok (1994a) presented a finite element analysis of an axially moving beam. This study was then continued by considering the effects of physical damping, tip mass, tip support, and wall flexibility on the stability characteristics of the aforementioned beam using the eigenvalue analysis (Stylianou and Tabarrok, 1994b). Raftoyiannis and Michaltsos (2013) employed a modal superposition technique for dynamic analysis of telescopic cranes' boom based on a continuum approach. Chang et al. (2010) used a finite element method to derive the equations of motion of an axially moving beam based on the Rayleigh beam theory. In this study, the stability of the beam with constant extension speed was sought using the eigenvalue analysis. Furthermore, the Floquet theory was employed to investigate the stability of the beam with periodical back-and-forth motion. Park et al. (2013) determined the dynamic behaviour of an axially moving

beam modelled by using the nonlinear von Karman strain theory. The results showed that the response of the system were consistent for both linear and nonlinear conditions. Furthermore, it was obtained that depending on the morphing acceleration and Young's modulus values, the differences between linear and nonlinear solutions might increase. Duan et al. (2014) studied the dynamic response of an axially moving nested beam theoretically and experimentally. The equations of motion were obtained using D'Alembert's principle and a good agreement between experimental and numerical results were obtained. The effects of a moving mass on the dynamic behavior of a two-stage telescopic mechanism used in truss structures of a bridge inspection vehicle was considered by Sui et al. (2015). In this research, the structural dynamics of the telescopic mechanism was modeled using Euler-Bernoulli beam theory. This study was then continued to investigate the dynamic behavior of a 2-DOF telescopic mechanism (Sui et al., 2016b). Yang et al. (2016) studied the energetics and invariants of the deploying beam with given initial conditions by the assumed-mode method. It was concluded that when the beam is being deployed with constant speed, the adiabatic invariant may be kept constant. Zhang et al. (2016) investigated the vibration characteristics of a Z-shaped beam with variable folding angles to model and design the Z-wing of a morphing aircraft. This study was then continued to investigate the nonlinear vibration behavior of a Z-shaped folded plate with inner resonance experimentally and numerically (Guo et al., 2019).

As it was mentioned above, the structural dynamics of the span morphing beam is dependent to its length, and hence the aeroelastic characteristics of telescopic wings can also be affected. Huang and Qiu (2013) studied the effects of span morphing velocities on the aeroelastic stability of a single variable-span with uniformity

assumption (uniform time invariant parameters). The established aeroelastic model was based on Euler-Bernoulli beam theory and unsteady vortex lattice aerodynamic theory. It was shown that using a span morphing mechanism can improve the aeroelastic performance of the wing. Zhang et al. (2013) investigated the nonlinear dynamic behaviour of a single deploying-and-retreating wing in supersonic airflow using a cantilevered laminated composite shell model. Also, Yang and Zhang (2014) studied the nonlinear vibrations of an axially moving beam by considering the coupling of the longitudinal and transversal motion. Zhang et al. (2014) investigated the nonlinear dynamics of a deploying orthotropic composite laminated cantilever rectangular plate with Reddy's third-order shear deformation plate and third-order nonlinear piston Theories. It was shown that deploying velocity and damping coefficients have great effects on the stability of system. This study was then developed further for subsonic airflow by combining the von Karman theory with Kutta-Joukowski lift theorem (Zhang et al., 2017). They characterized the effect of extension velocity on the nonlinear dynamic behaviour and stability of the wing. Lu et al. (2018) investigated the piezoelectric material characteristics and the time-varying nonlinear dynamic behavior of a deploying laminated composite plate under the aerodynamic loads and piezoelectric excitation. It was shown that by choosing a suitable voltage and polarity, the nonlinear vibration of the deploying cantilevered laminate can effectively be suppressed. Huang et al. (2018) studied the effects of rigid-body motions on the aeroelastic response of span-morphing wings. They combined Euler-Bernoulli beam theory with an unsteady strip aerodynamic theory and showed that the quasi static stability of the morphing wing is dependent on the fuselage flexibility. The flutter behavior of a variable-span wing in supersonic flow using the piston theory was considered by Li and Jin (2018). Ajaj and Friswell (2018) investigated the sensitivity of the flutter speed of a single variable-span morphing wing

for various system parameters and morphing velocities with uniformity assumption. They combined the shape functions of bending and torsional modes with the Theodorsen's unsteady aerodynamic model, and showed that the morphing speed affects the aeroelastic stability of the wing, and needs to be taken into account. The quasi static aeroelastic behaviour of telescopic, multi-segment, stepped, span morphing wings was studied by Ajaj et al. (2019). In this research, Euler-Bernoulli beam theory and Theodorsen's unsteady aerodynamic model were combined to form the aeroelastic equations. The results showed that this mechanism can be used as a means for wing flutter suppression. However, in their study, the effect of morphing speed was ignored.

In all previous studies concerned with the stability analysis of axially moving cantilever beams, several simplistic assumptions such as uniformity assumption and quasi-steady assumption were considered. Therefore, this study aims to offer a new aeroelastic framework for stability analysis of axially moving wings by removing all these simplistic assumptions. To this aim, the bending-torsional dynamics of the wing is modelled using Euler-Bernoulli beam theory, and the aerodynamic loads are simulated using Peters' unsteady aerodynamic model (Peters et al., 1995). The governing aeroelastic equations are discretized using a finite element method based on the beam-rod model. Finally, the effect of morphing speed and wing parameters on the length-based stability of the wing is determined by checking the eigenvalues of the system. It is noted that the main novelties of this paper are to investigate the effects of temporal variation of mass and length due to the movement of stages and their overlapping, along with the effects of morphing speed on the aeroelastic stability of two-stage telescopic wing with different properties.

Governing equations

As shown in Fig. 1, a two-stage Euler-Bernoulli beam model is employed to simulate the structural dynamics of an axially moving telescopic wing with sliding motion. The wing has an axially moving speed (morphing speed) of $\dot{\kappa}$, and the length of the fixed and moving parts are denoted by l_1 and l_m, respectively. The total time-dependent length, *l*, can be expressed as

$$l(t) = \dot{\kappa} t + l_1 \tag{1}$$

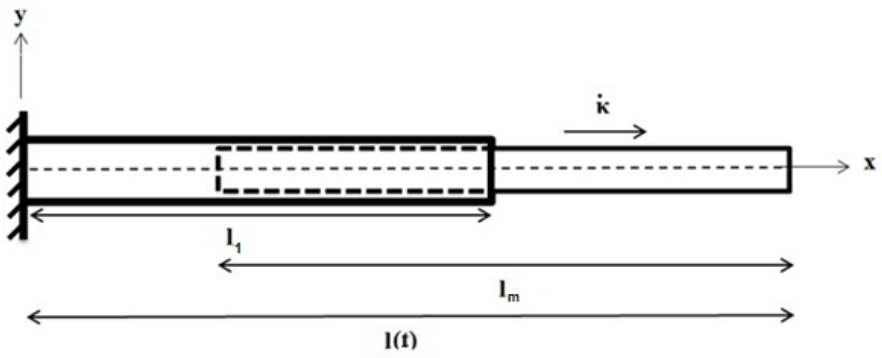

Fig. 1 Two-stage telescopic beam

The governing equations of motion are derived using the extended Hamilton's principle (Zhang and Qing, 2021) as follows

$$\delta \int_{t_1}^{t_2} (T - V + W)dt = 0 \tag{2}$$

where T , V and W are the kinetic energy, potential (strain) energy and nonconservative work, respectively.

Considering Fig. 1 as a two-stage telescopic wing, Fig. 2~~Fig. 2~~ shows a typical section of the wing including the out-of-plane bending (*h*) and the torsion (α) degrees of freedom.

Formatted: Font: 12 pt, Font color: Auto, Complex Script Font: 12 pt, Highlight

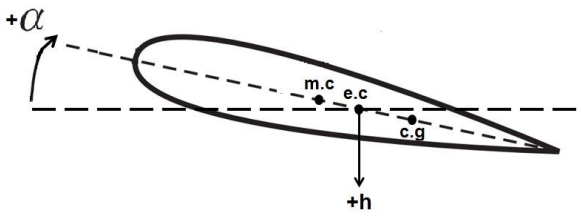

Fig. 2 Typical section of wing

The kinetic and potential energies of the wing can be expressed as

$$T = \frac{1}{2}\int_0^{l_1} m_1\left[\left(\frac{dh_1}{dt}+r_1\frac{d\alpha_1}{dt}\right)^2\right]dx + \frac{1}{2}\int_{l_1}^{l} m_2\left[\left(\frac{dh_2}{dt}+r_2\frac{d\alpha_2}{dt}\right)^2+\dot{\kappa}^2\right]dx$$

$$V = \frac{1}{2}\int_0^{l_1} EI_1\left(\frac{d^2h_1}{dx^2}\right)^2 dx + \frac{1}{2}\int_0^{l_1} GJ_1\left(\frac{d\alpha_1}{dx}\right)^2 dx + \frac{1}{2}\int_{l_1}^{l} EI_2\left(\frac{d^2h_2}{dx^2}\right)^2 dx + \frac{1}{2}\int_{l_1}^{l} GJ_2\left(\frac{d\alpha_2}{dx}\right)^2 dx + \int_0^{l_1} m_1 g\,(h_1+r_1\alpha_1)dx + \int_{l_1}^{l} m_2 g\,(h_2+r_2\alpha_2)dx \quad (3)$$

$$W = -F_e h_1(l_1,t) - F_e r_1 \alpha_1(l_1,t) + L h_1(x,t) + L h_2(x,t) + M\,\alpha_1(x,t) + M\,\alpha_2(x,t)$$

$$F_e = m_e(t)\left[g + \ddot{h}_1(l_1,t) + r_1\ddot{\alpha}_1(l_1,t)\right]$$

where m is the mass per length, EI is the bending rigidity and GJ is the torsional rigidity. Also, r is the distance between the center of mass and the elastic center, g is the acceleration of gravity, L is the aerodynamic force and M is the aerodynamic moment. Furthermore, the indices ($\bullet_1$) and ($\bullet_2$) refer to the fixed and moving parts of the wing, respectively. Also, $m_e(t)$ is the Equivalent mass at the end of the fixed part due to the incomplete connection of the moving part with the fixed part (Sui et al., 2016a):

$$m_e(t) = \frac{m_2\left[l_1^3 - (l(t) - l_m)^3\right]}{3l_1^2} \tag{4}$$

The first variation of kinetic and potential energies are defined as

$$\int_{t_1}^{t_2}(\delta T)dt = \int_0^{l_1}\int_{t_1}^{t_2} m_1\left[\frac{dh_1}{dt} + r_1\frac{d\alpha_1}{dt}\right]\left[\frac{d(\delta h_1)}{dt} + r_1\frac{d(\delta\alpha_1)}{dt}\right]dtdx +$$
$$+\int_{l_1}^{l}\int_{t_1}^{t_2} m_2\left[\frac{dh_2}{dt} + r_2\frac{d\alpha_2}{dt}\right]\left[\frac{d(\delta h_2)}{dt} + r\frac{d(\delta\alpha_2)}{dt}\right]dtdx + \int_{l_1}^{l}\int_{t_1}^{t_2} m_2\dot{\kappa}(\delta\dot{\kappa})dtdx$$

$$\int_{t_1}^{t_2}(\delta V)dt = \int_{t_1}^{t_2}\int_0^{l_1} EI_1\left(\frac{d^2h_1}{dx^2}\right)\delta\left(\frac{d^2h_1}{dx^2}\right)dx + \int_{t_1}^{t_2}\int_{l_1}^{l} EI_2\left(\frac{d^2h_2}{dx^2}\right)\delta\left(\frac{d^2h_2}{dx^2}\right)dx + \int_{t_1}^{t_2}\int_0^{l_1} GJ_1\left(\frac{d\alpha_1}{dx}\right)\delta\left(\frac{d\alpha_1}{dx}\right)dx +$$
$$+\int_{t_1}^{t_2}\int_{l_1}^{l} GJ_2\left(\frac{d\alpha_2}{dx}\right)\delta\left(\frac{d\alpha_2}{dx}\right)dx + \int_0^{l_1} m_1 g(\delta h_1 + r_1\delta\alpha_1)dx + \int_{l_1}^{l} m_2 g(\delta h_2 + r_2\delta\alpha_2)dx$$

$$\int_{t_1}^{t_2}(\delta W)dt = \int_{t_1}^{t_2}[L(\delta h_1 + \delta h_2) + M_{e.c}(\delta\alpha_1 + \delta\alpha_2) - \delta(F_e h_1(l_1,t)) - \delta(F_e r_1\alpha_1(l_1,t))]dt \tag{5}$$

By substituting Eq. 5 in Eq. 2, the general governing equations of motion for a two-stage wing can be obtained as follows

$$\left.\begin{aligned}&(m_1+m_e\delta(x-l_1))\left[\frac{d^2h_1}{dt^2}+g\right]+m_1r_1\frac{d^2\alpha_1}{dt^2}+\frac{d^2}{dx^2}(EI_1\frac{d^2h_1}{dx^2})=L\\&m_1(r_1^2\frac{d^2\alpha_1}{dt^2}+r_1g)+m_er_1\delta(x-l_1)\frac{d^2\alpha_1}{dt^2}+m_1r_1\frac{d^2h_1}{dt^2}-\frac{d}{dx}(GJ_1\frac{d\alpha_1}{dx})=M_{e.c}\end{aligned}\right\}\ 0<x<l_1$$

$$\left.\begin{aligned}&m_2(\frac{d^2h_2}{dt^2}+g)+m_2r_2\frac{d^2\alpha_2}{dt^2}+\frac{d^2}{dx^2}(EI_2\frac{d^2h_2}{dx^2})=L\\&m_2(r_2^2\frac{d^2\alpha_2}{dt^2}+r_2g)+m_2r_2\frac{d^2h_2}{dt^2}-\frac{d}{dx}(GJ_2\frac{d\alpha_2}{dx})=M_{e.c}\end{aligned}\right\}\ l_1<x<l \qquad (6)$$

As both bending and torsional variables are functions of time and space, and also due to the fact that $\dot{\kappa}=\frac{dl}{dt}=\frac{dx}{dt}$ the partial derivatives of each variable can be obtained as

$$\frac{dh}{dt}=\frac{\partial h}{\partial t}+\dot{\kappa}\frac{\partial h}{\partial x}$$

$$\frac{d\alpha}{dt}=\frac{\partial \alpha}{\partial t}+\dot{\kappa}\frac{\partial \alpha}{\partial x}$$

$$\frac{d^2h}{dt^2}=\frac{\partial^2 h}{\partial t^2}+2\dot{\kappa}\frac{\partial^2 h}{\partial x\,\partial t}+\dot{\kappa}^2\frac{\partial^2 h}{\partial x^2}+\ddot{\kappa}\frac{\partial h}{\partial x}$$

$$\frac{d^2\alpha}{dt^2}=\frac{\partial^2 \alpha}{\partial t^2}+2\dot{\kappa}\frac{\partial^2 \alpha}{\partial x\,\partial t}+\dot{\kappa}^2\frac{\partial^2 \alpha}{\partial x^2}+\ddot{\kappa}\frac{\partial \alpha}{\partial x} \qquad (7)$$

Finally, by substituting Eq. 7 in Eq. 6, and considering suitable bending and torsional shape functions ($H^h(x)$ and $H^\alpha(x)$) based on Hermitian beam element (Cook, 2007), the discretized weak form can be obtained (Appendix A).

The generalized lift and moment applied on the wing ($L^g, M^g_{e.c}$) are obtained using Peters' unsteady aerodynamic model as follows (Peters et al., 1995)

$$L = \pi\rho b^2(\ddot{h} + u\dot{\alpha} - ba\ddot{\alpha}) + 2\pi\rho ub(\dot{h} + u\alpha + b(\frac{1}{2} - a)\dot{\alpha} - \lambda_0)$$
$$M_{e.c} = M_{c/4} + b(0.5 + a)L$$
$$M_{c/4} = -\pi\rho b^3(\frac{1}{2}\ddot{h} + u\dot{\alpha} + b(\frac{1}{8} - \frac{a}{2})\ddot{\alpha})$$

$$\lambda_0 = \frac{1}{2}\sum_{n=1}^{N} b_{\text{inflow}}\lambda_n$$

$$[A_{\text{inflow}}]\{\dot{\lambda}_n\} + \frac{u}{b}\{\lambda_n\} = \{C_{\text{inflow}}\}[\ddot{h} + u\dot{\alpha} + b(0.5 - a)\ddot{\alpha}] \quad (8)$$

where u is the flight speed, b is the semi-chord, ρ is the air density, a is the nondimensional distance from the elastic center to the mid-chord, and the definitions of $[A_{\text{inflow}}]$, $\{C_{\text{inflow}}\}$ and $\{b_{\text{inflow}}\}$ are presented in the work of (Peters et al., 1995). It is noted that the discretized generalized aerodynamic lift and moment equations are given in Appendix A and related matrices are defined in the Appendix B.

The boundary conditions at the roots and the tips of the fixed and moving beams are listed as follows:

$$h_1(0,t) = 0, \quad \frac{\partial h_1}{\partial x}(0,t) = 0, \quad \alpha_1(0,t) = 0$$
$$EI_1\frac{\partial^2 h_1}{\partial x^2}(l_1,t) = EI_2\frac{\partial^2 h_2}{\partial x^2}(l_1,t), EI_1\frac{\partial^3 h_1}{\partial x^2}(l_1,t) = EI_2\frac{\partial^3 h_2}{\partial x^2}(l_1,t), GJ_1\frac{\partial \alpha_1}{\partial x}(l_1,t) = GJ_2\frac{\partial \alpha_2}{\partial x}(l_1,t)$$
$$EI_2\frac{\partial^2 h_2}{\partial x^2}(l,t) = 0, \quad EI_2\frac{\partial^3 h_2}{\partial x^2}(l,t) = 0, \quad GJ_2\frac{\partial \alpha_2}{\partial x}(l,t) = 0 \quad (9)$$

Finally, the discretized aeroelastic governing equations can be written in a compact form as follows

$$[M]\{\ddot{X}\}+[C]\{\dot{X}\}+[K]\{X\}=\{F\} \quad (10)$$

where **M**, **C** and **K** are the mass, damping and stiffness matrices, respectively.

It is ~~worth mentioning~~noted that the above general form of ~~the~~ aeroelastic equations contain the effects of length change and related parameters (such as morphing speed). As Fig. 3~~Fig. 3~~ shows, the dynamic instability onset of the system can be found by assuming the system morphs slowly, at any time during the length change, using ~~the~~ an eigenvalue analysis. This is referred to as the length-based stability analysis here which can be closer to the reality. It should be noted that the number of finite elements is fixed in time, and hence the size of the elements o~~f~~n the moving part changes at each time step.

Formatted: Font: 12 pt, Complex Script Font: 12 pt

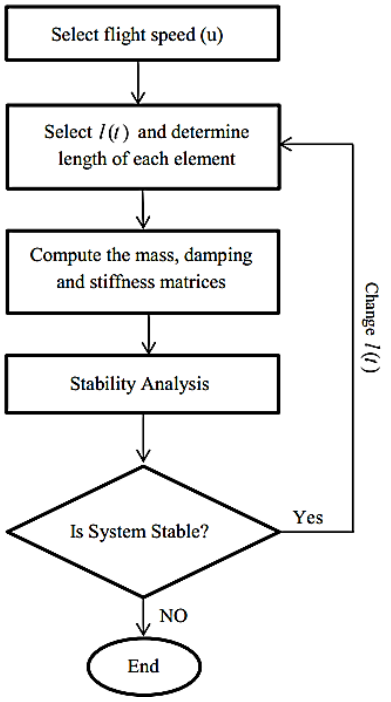

Fig. 3 Flowchart of stability analysis for the ~~two-stage~~two-stage morphing wing

2. Verification

To verify the developed model for morphing wings, first the time response of a two-stage Euler-Bernoulli telescopic beam subjected to a concentrated moving mass is obtained and compared with those reported by Sui et al. (2015), and shown in Fig. 4~~Fig. 4~~. The parameters used for this case are presented in Table 1~~Table 1~~. It is clear that the present results are in a good agreement with those presented by Sui et al. (2015) with maximum difference of 4%. It is noted that here 40 elements have been used for each of the fixed and the moving part, and the initial conditions are considered as compatible deformation with the presence of a concentrated mass (m_p) at the end of the beam.

Formatted: Font: 12 pt, Font color: Auto, Complex Script Font: 12 pt

Formatted: Font: 12 pt, Complex Script Font: 12 pt

Formatted: Font: 12 pt, Complex Script Font: 12 pt

Furthermore, here the effect of gravity is retained in the equations to be able to compare the results directly.

Table 1: Parameters of telescopic beams

Parameter	Value
l (m)	10.7
l_m (m)	10.7
m_1 (kg/m)	85
m_2 (kg/m)	46
EI_1 (Nm^2)	35
EI_2 (Nm^2)	35
$\dot{\kappa}$ (m/s)	0.5
m_p (kg)	400

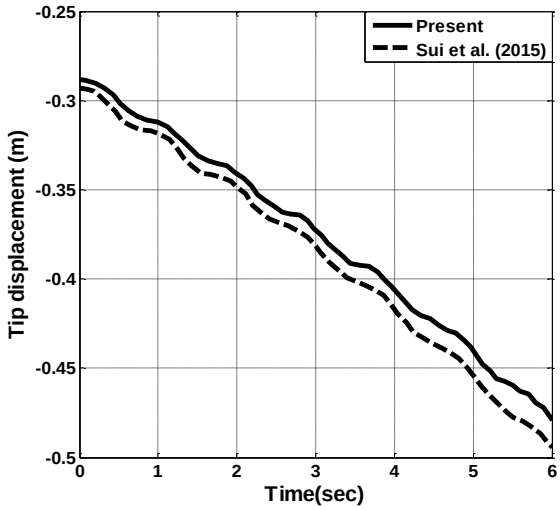

Fig. 4 The dynamic response of a two-stage telescopic beam subjected to a concentrated mass

Next, to verify the developed model for flutter analysis, a high aspect ratio wing with the properties defined in

Table 2~~Table 2~~ is used (Patil, 1999). It is noted that Patil (1999) solved the exact beam formulation using a finite element method. Furthermore, Ajaj et al. (2019) also analyzed the same wing based on Euler-Bernoulli beam structural model and Theodorsen's unsteady aerodynamic model using the Rayleigh-Ritz method. The flutter speed and frequency of this wing are obtained for two different numbers of elements, and compared with those calculated by Patil (1999) and Ajaj et al. (2019), and presented in

Table 3~~Table 3~~, and a very good agreement is observed.

Table 2: The high aspect ratio wing properties (Patil and Althoff, 2011)

Parameter	Value

Formatted: Font: 12 pt, Complex Script Font: 12 pt

Formatted: Font: 12 pt, Complex Script Font: 12 pt

l (m)	16
l_m (m)	8
c (m)	1
m_1 (kg/m)	0.75
EI_1 (Nm^2)	2 x 10^4
GJ_1 (Nm^2)	1 x 10^4
Spanwise elastic axis	50% chord
Center of gravity	50% chord
I (50%chord) (kg.m)	0.1

Table 3: The comparison of the flutter speed and frequency of the high aspect ratio wing

	Patil	Ajaj et al	Present method		Percent of Difference
			20 elements	40 elements	
$u_{flutter}$ (m/s)	32.21	33.43	33.6	33.45	0.06
$freq_{flutter}$ (rad/s)	22.61	21.38	21.5	21.73	1.63

Finally, the change of flutter speed of the telescopic wing with the properties presented in Table 2~~Table 2~~ are determined and compared with the results obtained by Ajaj et al. (2019) for two cases (quasi-static). The results are shown in Fig. 5~~Fig. 4~~, and a good

Formatted: Body, Justified, Line spacing: single, Don't keep with next

Formatted: Font: 12 pt, Complex Script Font: 12 pt

Formatted: Font: 12 pt, Complex Script Font: 12 pt

agreement is observed. It should be noted that using equivalent mass results in a reduction in computational time.

Furthermore, Fig. 6~~Fig. 5~~ shows the convergence of the flutter speed for the case of maximum length, for different numbers of elements. It is clear that by using 40 elements, the flutter speed can be predicted accurately, and hence from here on, 40 elements are used for all case studies.

Formatted: Font: 12 pt, Complex Script Font: 12 pt

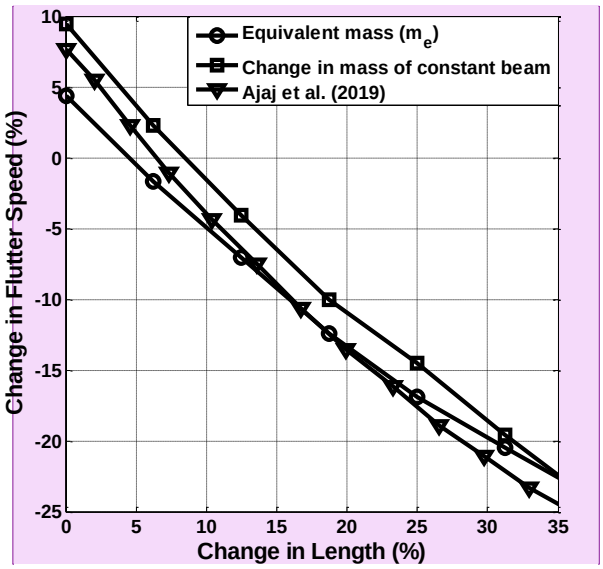

Fig. 5 The effect of wing span on the flutter speed for two mass models

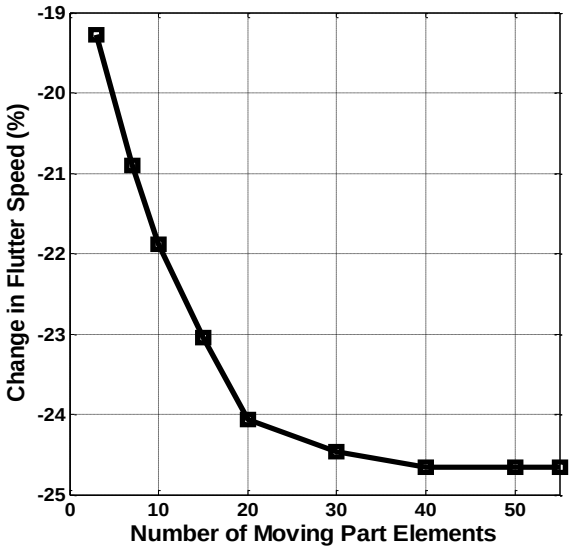

Fig. 6 The convergence of the flutter speed at maximum wing length

By considering all above studies, it can be concluded that the developed aeroelastic model is able to capture the aeroelastic stability of telescopic wings accurately. In what follows, the effects of various system parameters on the stability of telescopic wings are investigated.

3. Results

In the first step, the effect of wing length and morphing speed on the flutter speed is determined and shown in Fig. 7~~Fig. 6~~. Here, $\dot{\kappa} = 0$ refers to the quasi-static morphing in which the wing length increases at each stage, but related temporal changes in the coefficients of the equations are not taken into account. Fig. 7~~Fig. 6~~ shows that for the quasi-static morphing assumption ($\dot{\kappa} = 0$), a 37% increase in span length leads to a reduction of 28% in flutter speed. However, when the morphing speed is $\dot{\kappa} = 0.25$, the flutter speed reduces by up to 7%. This clearly shows that the morphing speed

Formatted: Not Highlight

Formatted: Not Highlight

significantly affects the flutter speed of the wing. It is also observed that ignoring the effect of mass of the moving part inside the fixed part (overlapping part) results in a change in flutter speed of up to 10%. This emphasizes the importance of the effect of overlapping part mass on the stability of the wing. Also, because the moving part slides inside the fixed part and the cross-section is fixed, the stiffness of the cross section is assumed to be constant.

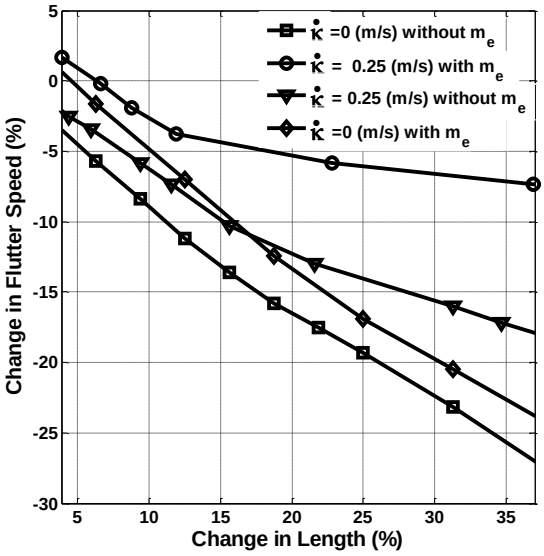

Fig. 7 The effect of wing span change and morphing speed on the flutter speed

In what follows, the critical length, (L_f), at which the wing gets unstable is obtained, and the effects of various system parameters on the sensitivity of the critical length are investigated.

3.1. Variation of mass per unit length

The effect of wing mass per unit length on the critical length of axially moving wings is determined and shown in Fig. 8~~Fig. 7~~. It is noted that unless otherwise stated, from here on all results are presented at a flight speed of 32 m/s and all values are nondimensionalized using the original wing parameters. Considering the effect of axially moving speed results in an improvement of up to 10% in the critical length compared to the original wing. Furthermore, the morphing wing critical length increases (decreases) when the mass per unit length increases (decreases). Also, the wing critical length is more sensitive to the mass per unit length of the fixed part than the moving part. Moreover, as shown in Fig. 8~~Fig. 7~~, the critical frequency of the morphing wing is also sensitive to the mass per unit length and morphing speed. The critical frequency is inversely related to the mass per unit length and moving speed. It is noted that the critical frequency is more sensitive to the mass per unit length than the morphing speed.

Formatted: Font: 12 pt, Complex Script Font: 12 pt

Formatted: Font: 12 pt, Font color: Auto, Complex Script Font: 12 pt

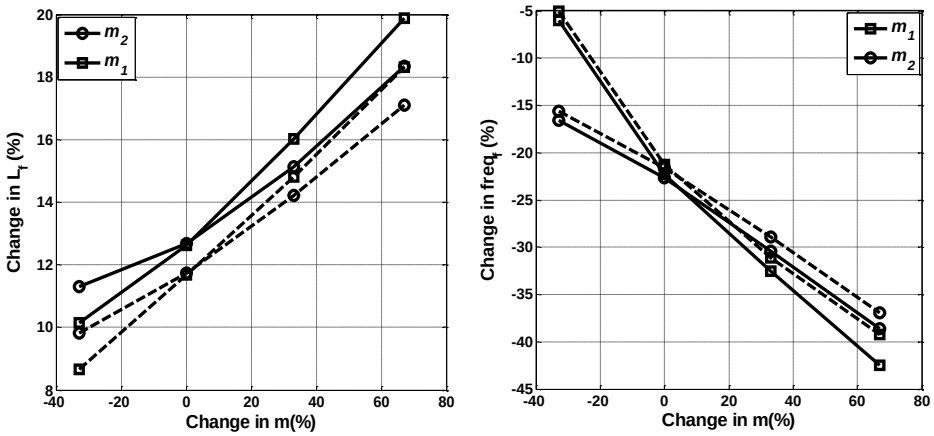

Fig. 8: The effect of mass per unit length and axially moving speed on the critical length and frequency of the wing (solid line $\dot{\kappa} = 1$ m/s, dashed line $\dot{\kappa} = 0.25$ m/s)

3.2. Variation of bending stiffness

Fig. 9~~Fig. 8~~ shows the effect of wing bending stiffness on the critical length for two different axially moving speeds. The wing critical length decreases when the bending stiffness increases. Furthermore, the bending stiffness of the fixed part affects the critical length more than the moving part. Moreover, the critical frequency and bending stiffness are directly related to each other, and hence an increase in bending stiffness results in an increase in the critical frequency.

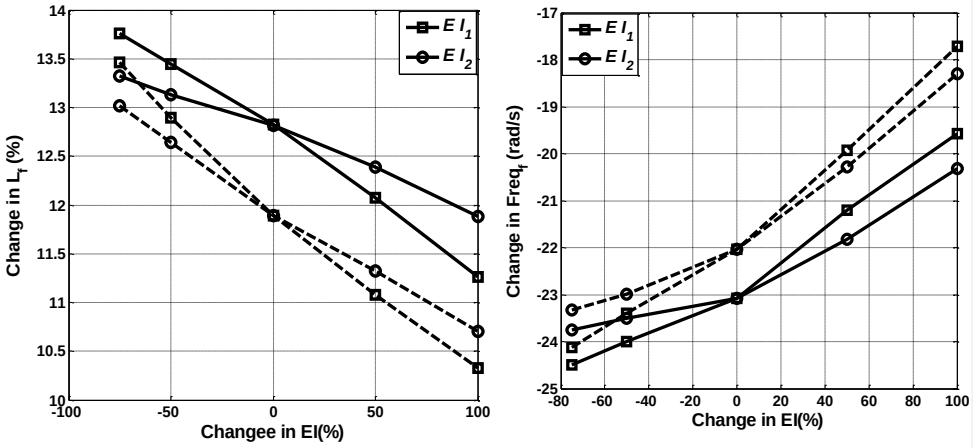

Fig. 9 The effect of bending stiffness and axially moving speed on the critical length and frequency of the wing (solid line $\dot{\kappa} = 1\ \mathrm{m/s}$, dashed line $\dot{\kappa} = 0.25\ \mathrm{m/s}$)

3.3. Variation of torsional stiffness

Fig. 10 ~~Fig. 9~~ shows the variation of critical length with respect to the change of torsional stiffness for two different axially moving speeds. The critical length increases when the torsional stiffness increases. It is noted that the torsional stiffness of the fixed part has higher impact on the critical length than the moving part. Moreover, the critical frequency and torsional stiffness are inversely related to each other. In this case, the

Formatted: Font: 12 pt, Complex Script Font: 12 pt

Formatted: Font: 12 pt, Complex Script Font: 12 pt

Formatted: Font: 12 pt, Complex Script Font: 12 pt

Formatted: Font: 12 pt, Complex Script Font: 12 pt

Formatted: Font: 12 pt, Complex Script Font: 12 pt

torsional stiffness has an effect of up to 40% on the critical length and up to 28% on the critical frequency.

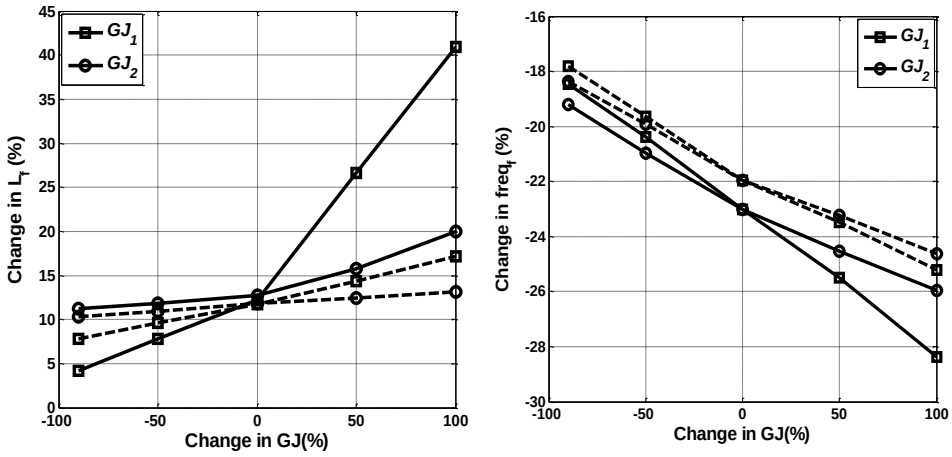

Fig. 10 The effect of torsional stiffness and axially moving speed on the critical length and frequency of the wing (solid line $\dot{\kappa} = 1\ \mathrm{m/s}$, dashed line $\dot{\kappa} = 0.25\ \mathrm{m/s}$)

Fig. 11~~Fig. 10~~ shows the effects of both bending stiffness and torsional stiffness on the wing critical length and frequency. It can be seen that at a certain morphing speed, torsional stiffness has a greater effect on the critical length. Furthermore, the wing critical length is more sensitive to the torsional stiffness of the fixed part than the moving part.

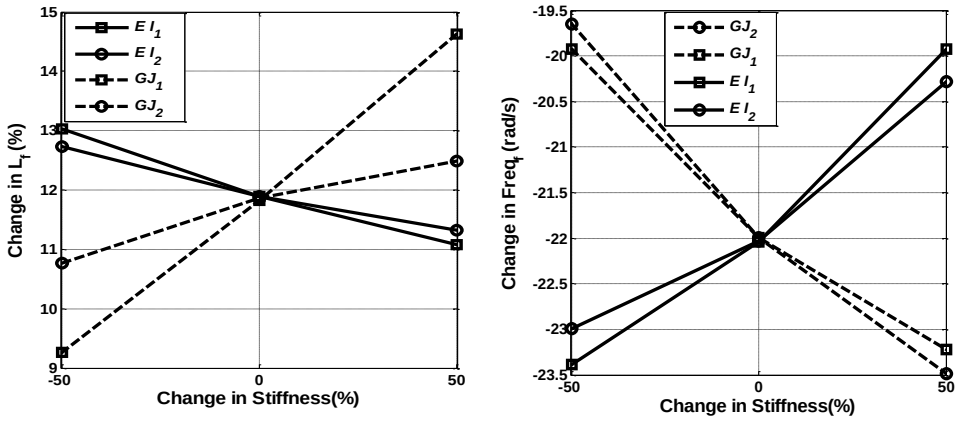

Fig. 11 The effect of bending and torsional stiffnesses on the critical length and frequency of the wing for $\dot{\kappa} = 0.25$ m/s

3.4. Variation of axially moving speed

The effect of axially moving speed on the critical length and frequency of the wing for various flight speeds is determined and shown in Fig. 12~~Fig. 11~~. By increasing the morphing speed, the critical length increases, while the critical frequency decreases. At first, both critical length and frequency change rapidly up to the axially moving speed of $\dot{\kappa}$=0.3 m/s, and then the rate of change reduces. This highlights that the morphing speed significantly affects the stability of the wing.

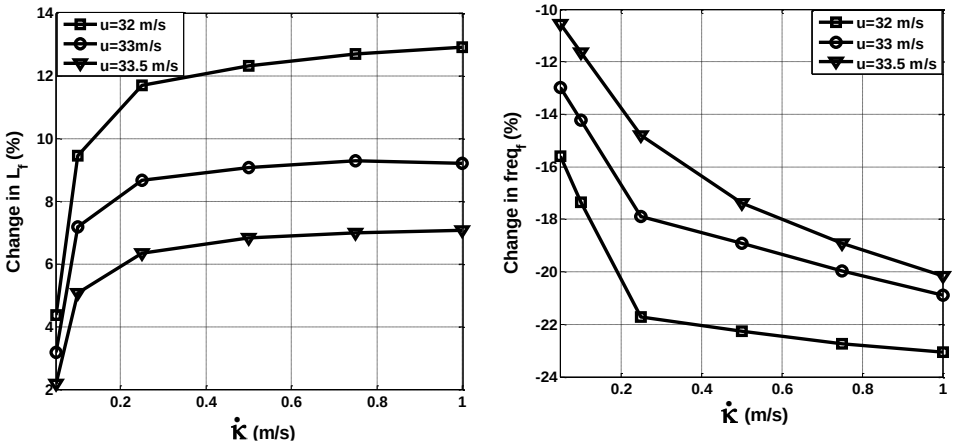

Fig. 12 The effect of axially moving speed on the critical length and frequency of the wing for various flight speeds

4. Conclusions

In this study, the aeroelastic stability of a conventional two-stage spanwise morphing UAV wing has been studied. The equations of motion have been obtained using the extended Hamilton's principle and discretized using the finite element method. The obtained results have been compared with those available in the literature, and a good agreement has been observed. The effect of morphing speed and wing parameters on the stability of the wing has been determined by checking the eigenvalues of the system. The results of this study are summarized as follows:

1- The aeroelastic stability of the telescopic wing is more sensitive to the fixed part parameters than the moving part.

2- The stability of the wing is more sensitive to the torsional stiffness than the bending stiffness.

3- The variation of the mass of the overlapped parts affects the aeroelastic stability of the wing.

4- The morphing speed has stabilizing effects.

Appendix A

substituting Eq. 7 in Eq. results in equation A.1

$$\left.\begin{aligned}
&(m_1+m_e\delta(x-l_1))\left[\frac{\partial^2 h_1}{\partial t^2}+g\right]+m_1 r_1\frac{\partial^2\alpha_1}{\partial t^2}+\frac{\partial^2}{\partial x^2}(EI_1\frac{\partial^2 h_1}{\partial x^2})=L\\
&m_1(r_1^2\frac{\partial^2\alpha_1}{\partial t^2}+r_1 g)+m_e r_1\delta(x-l_1)\frac{\partial^2\alpha_1}{\partial t^2}+m_1 r_1\frac{\partial^2 h_1}{\partial t^2}-\frac{\partial}{\partial x}(GJ_1\frac{\partial\alpha_1}{\partial x})=M_{e.c}
\end{aligned}\right\}\ 0<x<l_1$$

$$\left.\begin{aligned}
&m_2(\frac{\partial^2 h_2}{\partial t^2}+2\dot{\kappa}\frac{\partial^2 h_2}{\partial x\,\partial t}+\dot{\kappa}^2\frac{\partial^2 h_2}{\partial x^2}+\ddot{\kappa}\frac{\partial h_2}{\partial x}+g)+\\
&+m_2 r_2(\frac{\partial^2\alpha_2}{\partial t^2}+2\dot{\kappa}\frac{\partial^2\alpha_2}{\partial x\,\partial t}+\dot{\kappa}^2\frac{\partial^2\alpha_2}{\partial x^2}+\ddot{\kappa}\frac{\partial\alpha_2}{\partial x})+\frac{d^2}{dx^2}(EI_2\frac{d^2 h_2}{dx^2})=L\\
&m_2(r_2^2\left(\frac{\partial^2\alpha_2}{\partial t^2}+2\dot{\kappa}\frac{\partial^2\alpha_2}{\partial x\,\partial t}+\dot{\kappa}^2\frac{\partial^2\alpha_2}{\partial x^2}+\ddot{\kappa}\frac{\partial\alpha_2}{\partial x}\right)+r_2 g)+\\
&+m_2 r_2\left(\frac{\partial^2 h_2}{\partial t^2}+2\dot{\kappa}\frac{\partial^2 h_2}{\partial x\,\partial t}+\dot{\kappa}^2\frac{\partial^2 h_2}{\partial x^2}+\ddot{\kappa}\frac{\partial h_2}{\partial x}\right)-\frac{d}{dx}(GJ_2\frac{d\alpha_2}{dx})=M_{e.c}
\end{aligned}\right\}\ l_1<x<l$$

(A.1)

An example of obtaining the weak form based on A.1:

$$\left.\begin{aligned}
&m_2(\frac{\partial^2 h_2}{\partial t^2}+2\dot{\kappa}\frac{\partial^2 h_2}{\partial x\,\partial t}+\dot{\kappa}^2\frac{\partial^2 h_2}{\partial x^2}+\ddot{\kappa}\frac{\partial h_2}{\partial x}+g)+\\
&+m_2 r_2(\frac{\partial^2\alpha_2}{\partial t^2}+2\dot{\kappa}\frac{\partial^2\alpha_2}{\partial x\,\partial t}+\dot{\kappa}^2\frac{\partial^2\alpha_2}{\partial x^2}+\ddot{\kappa}\frac{\partial\alpha_2}{\partial x})+\frac{d^2}{dx^2}(EI_2\frac{d^2 h_2}{dx^2})=L
\end{aligned}\right\}\ l_1<x<l$$

(A.2)

$$h = [H^h]\{\delta h\}$$

$$\int_{l_1}^{l} [H^h]^T \begin{bmatrix} m_2(\frac{\partial^2 h_2}{\partial t^2} + 2\dot{\kappa}\frac{\partial^2 h_2}{\partial x\,\partial t} + \dot{\kappa}^2\frac{\partial^2 h_2}{\partial x^2} + \ddot{\kappa}\frac{\partial h_2}{\partial x} + g) + \\ + m_2 r_2(\frac{\partial^2 \alpha_2}{\partial t^2} + 2\dot{\kappa}\frac{\partial^2 \alpha_2}{\partial x\,\partial t} + \dot{\kappa}^2\frac{\partial^2 \alpha_2}{\partial x^2} + \ddot{\kappa}\frac{\partial \alpha_2}{\partial x}) + \frac{d^2}{dx^2}(EI_2\frac{d^2 h_2}{dx^2}) - L \end{bmatrix} dx =$$

$$\int_{l_1}^{l} \left[H^h\right]^T m_2(\frac{\partial^2 h_2}{\partial t^2})dx = \int_{l_1}^{l} m_2[H^h]^T[H^h]\{\delta\ddot{h}_2\}dx + \int_{l_1}^{l} m_2[H^h]^T(\frac{\partial^2[H^h]}{\partial t^2})\{\delta h_2\}dx + 2\int_{l_1}^{l} m_2[H^h]^T(\frac{\partial[H^h]}{\partial t})\{\delta\dot{h}_2\}$$

$$\int_{l_1}^{l} \left[H^h\right]^T 2\dot{\kappa}m_2\frac{\partial^2 h_2}{\partial x\,\partial t}dx = \int_{l_1}^{l} 2\dot{\kappa}m_2[H^h]^T(\frac{\partial^2[H^h]}{\partial x\,\partial t})\{\delta h_2\}dx + \int_{l_1}^{l} 2\dot{\kappa}m_2[H^h]^T\frac{\partial[H^h]}{\partial x}(\frac{\partial\{\delta h_2\}}{\partial t})dx$$

$$\int_{l_1}^{l} \left[H^h\right]^T m_2\dot{\kappa}^2\frac{\partial^2 h_2}{\partial x^2}dx = \int_{l_1}^{l} m_2\dot{\kappa}^2[H^h]^T\frac{\partial^2[H^h]}{\partial x^2}(\delta h_2)dx$$

$$\int_{l_1}^{l} \left[H^h\right]^T m_2\ddot{\kappa}\frac{\partial h_2}{\partial x}dx = \int_{l_1}^{l} m_2\ddot{\kappa}\left[H^h\right]^T\frac{\partial[H^h]}{\partial x}(\delta h_2)dx$$

$$\int_{l_1}^{l} \left[H^h\right]^T m_2 r_2(\frac{\partial^2 \alpha_2}{\partial t^2})dx = \int_{l_1}^{l} m_2 r_2[H^h]^T[H^h]\{\delta\ddot{\alpha}_2\}dx + \int_{l_1}^{l} m_2 r_2[H^h]^T(\frac{\partial^2[H^h]}{\partial t^2})\{\delta\alpha_2\}dx + 2\int_{l_1}^{l} m_2 r_2[H^h]^T(\frac{\partial[H^h]}{\partial t})\{\delta\dot{\alpha}_2\}$$

$$\int_{l_1}^{l} \left[H^h\right]^T 2\dot{\kappa}m_2 r_2\frac{\partial^2 \alpha_2}{\partial x\,\partial t}dx = \int_{l_1}^{l} 2\dot{\kappa}m_2 r_2[H^h]^T(\frac{\partial^2[H^h]}{\partial x\,\partial t})\{\delta\alpha_2\}dx + \int_{l_1}^{l} 2\dot{\kappa}m_2 r_2[H^h]^T\frac{\partial[H^h]}{\partial x}(\frac{\partial\{\delta\alpha_2\}}{\partial t})dx$$

$$\int_{l_1}^{l} \left[H^h\right]^T m_2 r_2\dot{\kappa}^2\frac{\partial^2 \alpha_2}{\partial x^2}dx = \int_{l_1}^{l} m_2 r_2\dot{\kappa}^2[H^h]^T\frac{\partial^2[H^h]}{\partial x^2}(\delta\alpha_2)dx$$

$$\int_{l_1}^{l} \left[H^h\right]^T m_2 r_2\ddot{\kappa}\frac{\partial \alpha_2}{\partial x}dx = \int_{l_1}^{l} m_2 r_2\ddot{\kappa}\left[H^h\right]^T\frac{\partial[H^h]}{\partial x}(\delta\alpha_2)dx$$

$$\int_{l_1}^{l} \left[H^h\right]^T \frac{d^2}{dx^2}(EI_2\frac{d^2 h_2}{dx^2})dx = EI_2\left[H^h\right]^T\frac{\partial^3 h_2}{\partial x^3}\Big]_{l_1}^{l} - EI_2\frac{\partial\left[H^h\right]^T}{\partial x}\frac{\partial^2 h_2}{\partial x^2}\Big]_{l_1}^{l} + \int_{l_1}^{l} EI_2\frac{\partial^2\left[H^h\right]^T}{\partial x^2}\frac{\partial^2\left[H^h\right]}{\partial x^2}\{\delta h_2\}dx$$

(A.3)

The weak form of Equation A.1 is obtained as A.4

$$\sum_{j=1}^{n_1}\begin{bmatrix} m_{ij}^{a}\ddot{h}_j + r\,m_{ij}^{b}\ddot{\alpha}_j + 2(c_{ij}^{a}+\dot{\kappa}c_{ij}^{b})\dot{h}_j + 2r(c_{ij}^{c}+\dot{\kappa}c_{ij}^{d})\dot{\alpha}_j + (k_{ij}^{a}+2\dot{\kappa}k_{ij}^{b}+\dot{\kappa}^2k_{ij}^{c}+\ddot{\kappa}k_{ij}^{d}+k_{ij}^{e})h_j + \\ +r(k_{ij}^{f}+2\dot{\kappa}k_{ij}^{g}+\dot{\kappa}^2k_{ij}^{h}+\ddot{\kappa}k_{ij}^{k})\alpha_j \end{bmatrix} = L^{g}$$

$$\sum_{n=1}^{n_1}\begin{bmatrix} r\,m_{mn}^{a}\ddot{h}_n + r^2 m_{mn}^{b}\ddot{\alpha}_n + 2r(c_{mn}^{a}+\dot{\kappa}c_{mn}^{b})\dot{h}_n + 2r^2(c_{mn}^{c}+\dot{\kappa}c_{mn}^{d})\dot{\alpha}_n + \\ +r(k_{mn}^{a}+2\dot{\kappa}k_{mn}^{b}+\dot{\kappa}^2k_{mn}^{c}+\ddot{\kappa}k_{mn}^{d})h_n + r^2(k_{mn}^{f}+2\dot{\kappa}k_{mn}^{g}+\dot{\kappa}^2k_{mn}^{o}+\ddot{\kappa}k_{mn}^{p}-k_{mn}^{e})\alpha_n \end{bmatrix} = M_{e.c}^{g}$$

$$\sum_{j=n_1+1}^{N}\begin{bmatrix} m_{ij}^{a}\ddot{h}_j + r\,m_{ij}^{b}\ddot{\alpha}_j + 2(c_{ij}^{a}+\dot{\kappa}c_{ij}^{b})\dot{h}_j + 2r(c_{ij}^{c}+\dot{\kappa}c_{ij}^{d})\dot{\alpha}_j + (k_{ij}^{a}+2\dot{\kappa}k_{ij}^{b}+\dot{\kappa}^2k_{ij}^{c}+\ddot{\kappa}k_{ij}^{d}+k_{ij}^{e})h_j + \\ +r(k_{ij}^{f}+2\dot{\kappa}k_{ij}^{g}+\dot{\kappa}^2k_{ij}^{h}+\ddot{\kappa}k_{ij}^{k})\alpha_j \end{bmatrix} = L^{g}$$

$$\sum_{n=n_1+1}^{N}\begin{bmatrix} r\,m_{mn}^{a}\ddot{h}_n + r^2 m_{mn}^{b}\ddot{\alpha}_n + 2r(c_{mn}^{a}+\dot{\kappa}c_{mn}^{b})\dot{h}_n + 2r^2(c_{mn}^{c}+\dot{\kappa}c_{mn}^{d})\dot{\alpha}_n + \\ +r(k_{mn}^{a}+2\dot{\kappa}k_{mn}^{b}+\dot{\kappa}^2k_{mn}^{c}+\ddot{\kappa}k_{mn}^{d})h_n + r^2(k_{mn}^{f}+2\dot{\kappa}k_{mn}^{g}+\dot{\kappa}^2k_{mn}^{o}+\ddot{\kappa}k_{mn}^{p}-k_{mn}^{e})\alpha_n \end{bmatrix} = M_{e.c}^{g}$$

(A.4)

Also, the weak form of aerodynamic equations can be written as

$$L^{g} = \sum_{j=1}^{n}\begin{Bmatrix} \pi\rho b^2[m_{ij}^{c}\ddot{h}_j - ba\,m_{ij}^{d}\ddot{\alpha}_j + 2(c_{ij}^{e}+\dot{\kappa}c_{ij}^{f})\dot{h}_j - 2ba(c_{ij}^{g}+\dot{\kappa}c_{ij}^{p})\dot{\alpha}_j \\ +u\,c_{ij}^{q}\dot{\alpha}_j + (k_{ij}^{l}+2\dot{\kappa}k_{ij}^{o}+\dot{\kappa}^2k_{ij}^{p}+\ddot{\kappa}k_{ij}^{q})h_j \\ -ba(k_{ij}^{r}+2\dot{\kappa}k_{ij}^{s}+\dot{\kappa}^2k_{ij}^{t}+\ddot{\kappa}k_{ij}^{u})\alpha_j + u(k_{ij}^{v}+k_{ij}^{w})\alpha_j] + \\ +2\pi\rho ub(c_{ij}^{r}\dot{h}_j + b(\frac{1}{2}-a)c_{ij}^{q}\dot{\alpha}_j + (k_{ij}^{y}+k_{ij}^{z})h_j + uk_{ij}^{x}\alpha_j + b(\frac{1}{2}-a)(k_{ij}^{v}+k_{ij}^{w})\alpha_j - \lambda_0) \end{Bmatrix}$$

$$M_{c/4}^{g} = -\pi\rho b^3\sum_{n=1}^{N}\begin{Bmatrix} \frac{1}{2}m_{mn}^{c}\ddot{h}_n + b(\frac{1}{8}-\frac{a}{2})m_{mn}^{d}\ddot{\alpha}_n + (c_{mn}^{e}+\dot{\kappa}c_{mn}^{f})\dot{h}_n + b(\frac{1}{4}-a)(c_{mn}^{g}+\dot{\kappa}c_{mn}^{p})\dot{\alpha}_n \\ +u\,c_{mn}^{q}\dot{\alpha}_n + \frac{1}{2}(k_{mn}^{l}+2\dot{\kappa}k_{mn}^{o}+\dot{\kappa}^2k_{mn}^{p}+\ddot{\kappa}k_{mn}^{q})h_n \\ +b(\frac{1}{8}-\frac{a}{2})(k_{mn}^{r}+2\dot{\kappa}k_{mn}^{s}+\dot{\kappa}^2k_{mn}^{t}+\ddot{\kappa}k_{mn}^{u})\alpha_n + u(k_{mn}^{v}+k_{mn}^{w})\alpha_n \end{Bmatrix}$$

(A.5)

Appendix B

$$m_{ij}^{a} = m\int_{x_j}^{x_{j+1}} H_i^h H_j^h dx \qquad m_{mn}^{a} = m\int_{x_n}^{x_{n+1}} H_m^\alpha H_n^h dx \qquad m_{ij}^{c} = \int_{x_j}^{x_{j+1}} H_i^h H_j^h dx \qquad m_{mn}^{c} = \int_{x_n}^{x_{n+1}} H_m^\alpha H_n^h dx$$

$$c_{ij}^{a} = m\int_{x_j}^{x_{j+1}} H_i^h \dot{H}_j^h dx \qquad c_{mn}^{a} = m\int_{x_n}^{x_{n+1}} H_m^\alpha \dot{H}_n^h dx \qquad c_{ij}^{e} = \int_{x_j}^{x_{j+1}} H_i^h \dot{H}_j^h dx \qquad c_{mn}^{e} = \int_{x_n}^{x_{n+1}} H_m^\alpha \dot{H}_n^h dx$$

$$c_{ij}^{b} = m\int_{x_j}^{x_{j+1}} H_i^h H_j'^h dx \qquad c_{mn}^{b} = m\int_{x_n}^{x_{n+1}} H_m^\alpha H_n'^h dx \qquad c_{ij}^{f} = \int_{x_j}^{x_{j+1}} H_i^h H_j'^h dx \qquad c_{mn}^{f} = \int_{x_n}^{x_{n+1}} H_m^\alpha H_n'^h dx$$

$$k_{ij}^{a} = m\int_{x_j}^{x_{j+1}} H_i^h \ddot{H}_j^h dx \qquad k_{mn}^{a} = m\int_{x_n}^{x_{n+1}} H_m^\alpha \ddot{H}_n^h dx \qquad k_{ij}^{l} = \int_{x_j}^{x_{j+1}} H_i^h \ddot{H}_j^h dx \qquad k_{mn}^{l} = \int_{x_n}^{x_{n+1}} H_m^\alpha \ddot{H}_n^h dx$$

$$k_{ij}^{b} = m\int_{x_j}^{x_{j+1}} H_i^h \dot{H}_j'^h dx \qquad k_{mn}^{b} = m\int_{x_n}^{x_{n+1}} H_m^\alpha \dot{H}_n'^h dx \qquad k_{ij}^{o} = \int_{x_j}^{x_{j+1}} H_i^h \dot{H}_j'^h dx \qquad k_{mn}^{o} = \int_{x_n}^{x_{n+1}} H_m^\alpha \dot{H}_n'^h dx$$

$$k_{ij}^{c} = m\int_{x_j}^{x_{j+1}} H_i^h H_j''^h dx \qquad k_{mn}^{c} = m\int_{x_n}^{x_{n+1}} H_m^\alpha H_n''^h dx \qquad k_{ij}^{p} = \int_{x_j}^{x_{j+1}} H_i^h H_j''^h dx \qquad k_{mn}^{p} = \int_{x_n}^{x_{n+1}} H_m^\alpha H_n''^h dx$$

$$k_{ij}^{d} = m\int_{x_j}^{x_{j+1}} H_i^h H_j'^h dx \qquad k_{mn}^{d} = m\int_{x_n}^{x_{n+1}} H_m^\alpha H_n'^h dx \qquad k_{ij}^{q} = \int_{x_j}^{x_{j+1}} H_i^h H_j'^h dx \qquad k_{mn}^{q} = \int_{x_n}^{x_{n+1}} H_m^\alpha H_n'^h dx$$

$$m_{ij}^{b} = m\int_{x_j}^{x_{j+1}} H_i^h H_j^\alpha dx \qquad m_{mn}^{b} = m\int_{x_n}^{x_{n+1}} H_m^\alpha H_n^\alpha dx \qquad m_{ij}^{d} = \int_{x_j}^{x_{j+1}} H_i^h H_j^\alpha dx \qquad m_{mn}^{d} = \int_{x_n}^{x_{n+1}} H_m^\alpha H_n^\alpha dx$$

$$c_{ij}^{c} = m\int_{x_j}^{x_{j+1}} H_i^h \dot{H}_j^\alpha dx \qquad c_{mn}^{c} = m\int_{x_n}^{x_{n+1}} H_m^\alpha \dot{H}_n^\alpha dx \qquad c_{ij}^{g} = \int_{x_j}^{x_{j+1}} H_i^h \dot{H}_j^\alpha dx \qquad c_{mn}^{g} = \int_{x_n}^{x_{n+1}} H_m^\alpha \dot{H}_n^\alpha dx$$

$$c_{ij}^{d} = m\int_{x_j}^{x_{j+1}} H_i^h H_j'^\alpha dx \qquad c_{mn}^{d} = m\int_{x_n}^{x_{n+1}} H_m^\alpha H_n'^\alpha dx \qquad c_{ij}^{p} = \int_{x_j}^{x_{j+1}} H_i^h H_j'^\alpha dx \qquad c_{mn}^{p} = \int_{x_n}^{x_{n+1}} H_m^\alpha H_n'^\alpha dx$$

$$k_{ij}^{f} = m\int_{x_j}^{x_{j+1}} H_i^h \ddot{H}_j^\alpha dx \qquad k_{mn}^{f} = m\int_{x_n}^{x_{n+1}} H_m^\alpha \ddot{H}_n^\alpha dx \qquad c_{ij}^{q} = \int_{x_j}^{x_{j+1}} H_i^h H_j^\alpha dx \qquad c_{mn}^{q} = \int_{x_n}^{x_{n+1}} H_m^\alpha H_n^\alpha dx$$

$$k_{ij}^{g} = m\int_{x_j}^{x_{j+1}} H_i^h \dot{H}_j'^\alpha dx \qquad c_{ij}^{r} = \int_{x_j}^{x_{j+1}} H_i^h H_j^h dx \qquad k_{mn}^{r} = \int_{x_n}^{x_{n+1}} H_m^\alpha \ddot{H}_n^\alpha dx$$

$$k_{ij}^{h} = m\int_{x_j}^{x_{j+1}} H_i^{h} H_j''^{\alpha} dx \qquad k_{mn}^{g} = m\int_{x_n}^{x_{n+1}} H_m^{\alpha} \dot{H}_n'^{\alpha} dx \qquad k_{ij}^{r} = \int_{x_j}^{x_{j+1}} H_i^{h} \ddot{H}_j^{\alpha} dx \qquad k_{mn}^{s} = \int_{x_n}^{x_{n+1}} H_m^{\alpha} \dot{H}_n'^{\alpha} dx$$

$$k_{ij}^{k} = m\int_{x_j}^{x_{j+1}} H_i^{h} H_j'^{\alpha} dx \qquad k_{mn}^{o} = m\int_{x_n}^{x_{n+1}} H_m^{\alpha} H_n''^{\alpha} dx \qquad k_{ij}^{s} = \int_{x_j}^{x_{j+1}} H_i^{h} \dot{H}_j'^{\alpha} dx \qquad k_{mn}^{t} = \int_{x_n}^{x_{n+1}} H_m^{\alpha} H_n''^{\alpha} dx$$

$$k_{mn}^{p} = m\int_{x_n}^{x_{n+1}} H_m^{\alpha} H_n'^{\alpha} dx$$

$$k_{ij}^{e} = EI\int_{x_j}^{x_{j+1}} H_i'''^{h} H_j''^{h} dx \qquad k_{ij}^{t} = \int_{x_j}^{x_{j+1}} H_i^{h} H_j''^{\alpha} dx \qquad k_{mn}^{u} = \int_{x_n}^{x_{n+1}} H_m^{\alpha} H_n'^{\alpha} dx$$

$$k_{ij}^{u} = \int_{x_j}^{x_{j+1}} H_i^{h} H_j'^{\alpha} dx \qquad k_{mn}^{e} = GJ\int_{x_n}^{x_{n+1}} H_i'^{\alpha} H_j'^{\alpha} dx \qquad k_{ij}^{w} = \int_{x_j}^{x_{j+1}} H_i^{h} H_j'^{\alpha} dx \qquad k_{ij}^{x} = \int_{x_j}^{x_{j+1}} H_i^{h} H_j^{\alpha} dx$$

$$k_{ij}^{v} = \int_{x_j}^{x_{j+1}} H_i^{h} \dot{H}_j^{\alpha} dx$$

$$k_{ij}^{y} = \int_{x_j}^{x_{j+1}} H_i^{h} \dot{H}_j^{h} dx$$

$$k_{ij}^{z} = \int_{x_j}^{x_{j+1}} H_i^{h} H_j'^{h} dx$$

Declaration of conflicting interests

The authors declare no conflict of interest in preparing this article.

Funding

This research received no specific grant from any funding agency in the public, commercial, or not-for-profit sectors.

References

Ajaj RM and Friswell MI. (2018) Aeroelasticity of compliant span morphing wings. *Smart materials and structures* 27: 105052.

Ajaj RM, Omar FK, Darabseh TT, et al. (2019) Flutter of telescopic span morphing wings. *International Journal of Structural Stability and Dynamics* 19: 1950061.

Bisplinghoff RL, Ashley H and Halfman RL. (2013) *Aeroelasticity*: Courier Corporation.

Chang J-R, Lin W-J, Huang C-J, et al. (2010) Vibration and stability of an axially moving Rayleigh beam. *Applied Mathematical Modelling* 34: 1482-1497.

Cook RD. (2007) *Concepts and applications of finite element analysis*: John wiley & sons.

Duan Y-C, Wang J-P, Wang J-Q, et al. (2014) Theoretical and experimental study on the transverse vibration properties of an axially moving nested cantilever beam. *Journal of Sound and Vibration* 333: 2885-2897.
Friswell MI and Inman DJ. (2006) Morphing concepts for UAVs. *21st Bristol UAV systems conference.* 13.11-13.18.
Guo X, Zhang Y, Zhang W, et al. (2019) Theoretical and experimental investigation on the nonlinear vibration behavior of Z-shaped folded plates with inner resonance. *Engineering Structures* 182: 123-140.
Huang C, Chao Y, Zhigang W, et al. (2018) Variations of flutter mechanism of a span-morphing wing involving rigid-body motions. *Chinese Journal of Aeronautics* 31: 490-497.
Huang R and Qiu Z. (2013) Transient aeroelastic responses and flutter analysis of a variable-span wing during the morphing process. *Chinese Journal of Aeronautics* 26: 1430-1438.
Li W and Jin D. (2018) Flutter suppression and stability analysis for a variable-span wing via morphing technology. *Journal of Sound and Vibration* 412: 410-423.
Lu S, Zhang W and Song X. (2018) Time-varying nonlinear dynamics of a deploying piezoelectric laminated composite plate under aerodynamic force. *Acta Mechanica Sinica* 34: 303-314.
Park S, Yoo HH and Chung J. (2013) Vibrations of an axially moving beam with deployment or retraction. *AIAA journal* 51: 686-696.
Patil MJ. (1999) *Nonlinear aeroelastic analysis, flight dynamics, and control of a complete aircraft*: Georgia Institute of Technology.
Patil MJ and Althoff M. (2011) Energy-consistent, Galerkin approach for the nonlinear dynamics of beams using intrinsic equations. *Journal of Vibration and Control* 17: 1748-1758.
Peters DA, Karunamoorthy S and Cao W-M. (1995) Finite state induced flow models. I-Two-dimensional thin airfoil. *Journal of aircraft* 32: 313-322.
Raftoyiannis IG and Michaltsos GT. (2013) Dynamic behavior of telescopic cranes boom. *International Journal of Structural Stability and Dynamics* 13: 1350010.
Stylianou M and Tabarrok B. (1994a) Finite element analysis of an axially moving beam, part I: time integration. *Journal of Sound and Vibration* 178: 433-453.
Stylianou M and Tabarrok B. (1994b) Finite element analysis of an axially moving beam, part II: stability analysis. *Journal of Sound and Vibration* 178: 455-481.
Sui W, Zhu Z and Cao G. (2015) Dynamic responses of axially moving telescopic mechanism for truss structure bridge inspection vehicle under moving mass. *Journal of Vibroengineering* 18: 408-416.
Sui W, Zhu Z, Cao G, et al. (2016a) 1959. Dynamic behaviors of 2-DOF axially telescopic mechanism for truss structure bridge inspection vehicle. *Journal of Vibroengineering* 18.
Sui W, Zhu Z, Cao G, et al. (2016b) Dynamic behaviors of 2-DOF axially telescopic mechanism for truss structure bridge inspection vehicle. *Journal of Vibroengineering* 18: 1145-1156.
Wang PKC and Wei J-D. (1987) Vibrations in a moving flexible robot arm. *Journal of Sound Vibration* 116: 149-160.
Yang X-D and Zhang W. (2014) Nonlinear dynamics of axially moving beam with coupled longitudinal–transversal vibrations. *Nonlinear Dynamics* 78: 2547-2556.
Yang X-D, Zhang W and Melnik RV. (2016) Energetics and invariants of axially deploying beam with uniform velocity. *AIAA Journal* 54: 2183-2189.
Zhang P and Qing H. (2021) Free vibration analysis of Euler–Bernoulli curved beams using two-phase nonlocal integral models. *Journal of Vibration and Control*: 10775463211022483.
Zhang W, Chen L-L, Guo X-Y, et al. (2017) Nonlinear dynamical behaviors of deploying wings in subsonic air flow. *Journal of Fluids and Structures* 74: 340-355.
Zhang W, Hu W, Cao D, et al. (2016) Vibration frequencies and modes of a z-shaped beam with variable folding angles. *Journal of Vibration and Acoustics* 138.
Zhang W, Lu S and Yang X. (2014) Analysis on nonlinear dynamics of a deploying composite laminated cantilever plate. *Nonlinear Dynamics* 76: 69-93.

Zhang W, Sun L, Yang X, et al. (2013) Nonlinear dynamic behaviors of a deploying-and-retreating wing with varying velocity. *Journal of Sound and Vibration* 332: 6785-6797.